J. Fluid Mech. (2024), *vol*. 984, A21, doi:10.1017/jfm.2024.219

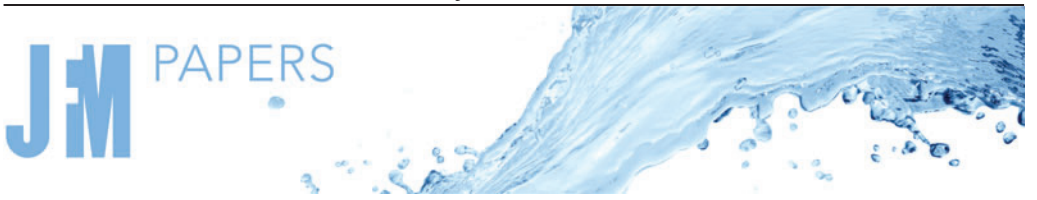

A PINN approach for identifying governing parameters of noisy thermoacoustic systems

Hwijae Son[1] **and Minwoo Lee**[2],†

[1]Department of Mathematics, Konkuk University, 120 Neungdongro, Gwangjin, Seoul 05029, South Korea

[2]Department of Mechanical Engineering, Hanbat National University, 125 Dongseodaero, Yuseong, Daejeon 34158, South Korea

(Received 30 October 2023; revised 11 January 2024; accepted 27 February 2024)

Identifying the governing parameters of self-sustained oscillation is crucial for the diagnosis, prediction and control of thermoacoustic instabilities. In this paper, we propose and validate a novel method for computing the parameters of thermoacoustic oscillation in a stochastic environment, which exploits a physics-informed neural network (PINN). Specifically, we introduce a negative log-likelihood loss function that integrates the stochastic samples and the solution of the Fokker–Planck equation. The proposed framework is validated using the numerically generated signal and the experimental data obtained from an annular combustor, both before and after the supercritical Hopf bifurcation. The results of PINN-based system identification show good agreement with the actual system parameters and the original stochastic signal, with improved accuracy compared to established methods. To the best of our knowledge, this study constitutes the first demonstration of the PINN-inverse approach that uses the noise-induced dynamics of thermoacoustic systems, opening up new pathways for diagnosing and predicting the thermoacoustic behaviour of various combustion systems.

Key words: machine learning, low-dimensional models, combustion

1. Introduction

1.1. *Thermoacoustic oscillations via Hopf bifurcation*

Despite extensive research spanning many decades, thermoacoustic oscillations remain a critical issue in developing and operating combustion systems such as rocket and gas turbine combustors. These oscillations occur from the positive feedback loop between the heat-release-rate fluctuations of an unsteady flame and the acoustic oscillations within the combustor (Lieuwen & Yang 2005). When these two types of oscillations align

† Email address for correspondence: mwlee@hanbat.ac.kr

in phase, self-sustained thermoacoustic instability arises at one or more of the natural acoustic frequencies of the combustor via the Rayleigh mechanism (Magri, Juniper & Moeck 2020). In most cases, thermoacoustic oscillation is considered undesirable, as it exerts thermal stress on the combustion devices, potentially leading to mechanical damage or failure. Therefore, diagnosing the combustion system in terms of thermoacoustic instability is crucial in combustion systems so as to control the oscillation and prevent the pressure surge (Juniper & Sujith 2018; Krishnan *et al.* 2021).

Phenomenologically, birth and extinction of a thermoacoustic oscillation is often characterized as a Hopf bifurcation occurring between the fixed point and the limit cycle (Noiray & Schuermans 2013; Subramanian, Sujith & Wahi 2013). The normal form of the Hopf bifurcation in a nonlinear oscillating system is

$$\frac{\mathrm{d}a}{\mathrm{d}t} = k_1 a + k_2 a\,|a|^2, \tag{1.1}$$

where $a = |a|\,\mathrm{e}^{\mathrm{i}\phi}$ is the amplitude of oscillation, t is time, ϕ is phase, and k_1 and k_2 are linear growth rate and nonlinear parameter, respectively. Negative and positive values of k_1 indicate fixed-point and limit-cycle regimes, respectively, with the Hopf bifurcation occurring at $k_1 = 0$ (Hopf point). Also, the negative nonlinear parameter ($k_2 < 0$) results in a supercritical Hopf bifurcation, where the limit cycle is observed only after the Hopf point ($k_1 > 0$). On the contrary, when k_2 is positive, subcritical Hopf bifurcation occurs, and the limit cycle can take place even at negative k_1. One or more higher-order nonlinear terms may be required to stabilize the oscillation in the latter situation. It is worth mentioning that in the hydrodynamics community, (1.1) is known as the Stuart–Landau equation (Landau 1944; Stuart 1960) characterizing the hydrodynamic instabilities in various types of flows, e.g. low-density jets (Raghu & Monkewitz 1991).

1.2. *System identification using noise-induced dynamics for the diagnosis of thermoacoustic oscillations*

When the amplitude oscillation in a thermoacoustic system is modelled with (1.1), it is crucial to identify the linear and nonlinear system parameters. In particular, the system parameters succinctly express the thermoacoustic dynamics, thus the system can be diagnosed using these values. The computation of system parameters can be conducted via system identification, which involves statistical analysis of the system's output signal. An established method of system identification near a Hopf bifurcation uses the noise-induced dynamics (NID) of the system (Lee *et al.* 2019; Kabiraj, Vishnoi & Saurabh 2020). Opposing the conventional view of regarding noise as a signal contamination, researchers have shown that a stochastically perturbed system can reveal more information about its original deterministic dynamics than a noise-free system via the NID (Pikovsky & Kurths 1997; Ushakov *et al.* 2005; Kabiraj *et al.* 2015). Therefore, in the system identification framework mentioned above, a stochastic differential equation (SDE) is postulated to capture the noise-induced behaviour of the system. Near the Hopf point where the growth rate is small, the system is weakly nonlinear, and the stochastic averaging can be applied to this SDE, yielding an equivalent Fokker–Planck equation describing the drift and diffusion dynamics of the thermoacoustic system. Siegert, Friedrich & Peinke (1998) have proposed that drift and diffusion terms of the Fokker–Planck equation can be extracted by analysing the time correlation of the noisy data, establishing an output-only system identification method. Noiray & Schuermans (2013) first applied this framework to compute linear and nonlinear parameters of the stochastic Van der

Pol equation governing thermoacoustic oscillations in a gas-turbine combustor. Noiray & Denisov (2017) later validated this stochastic system identification framework by applying periodic feedback control to the combustor at both the stable and unstable regimes. Consequently, the system identification method using the stochastic Van der Pol equation and the corresponding Fokker–Planck equation is applied to numerous combustion systems exhibiting thermoacoustic oscillation, including both laminar and turbulent combustors (Boujo & Noiray 2017; Bonciolini, Boujo & Noiray 2017; Lee *et al.* 2020, 2021).

Despite the robustness of the NID-based system identification framework proven in various thermoacoustic systems, there exists an intrinsic limitation that hinders the accuracy of the extracted parameters. First, established methods of system identification that exploit the NID of the system are based on the probability mass function, counting discrete samples of the time-shifted signal. This causes the inherent discrete approximation error, especially when the input sample size is small. Furthermore, while computing the time correlation of the signal, the noise is assumed to be perfectly memoryless. In practical thermoacoustic systems, however, Markovian assumption can be severely impaired due to the coarse sampling rate and the signal filtering. In such situations, adverse finite-time effects arise, and further adjustment of the computed parameters may be required, specifically by incorporating the optimization scheme based on adjoint equations (Lade 2009; Boujo & Noiray 2017; Lee, Kim & Park 2023*b*). To the best of our knowledge, a NID-based system identification method that is unaffected by the above-mentioned limitations due to discrete time-shift computation has yet to be developed.

1.3. *Physics-informed neural networks for the system identification of thermoacoustic systems*

Along with recent advances in machine learning, neural networks are increasingly applied for the analysis of thermoacoustic systems. Selimefendigil & Polifke (2011) developed a low-order model in the frequency domain for predicting thermoacoustic limit cycles using the feed-forward neural network identification method. Consequently, neural networks are exploited for deducing heat release models (Jaensch & Polifke 2017) and nonlinear flame responses (Tathawadekar *et al.* 2021) in thermoacoustic systems. Recently, Nóvoa & Magri (2022) used an echo state network, a reservoir-computing-based recurrent neural network, for the real-time bias-aware estimation of the states and parameters of a numerical Rijke tube model. Nóvoa, Racca & Magri (2024) later generalized this echo state network with a regularized bias-aware ensemble Kalman filter. Building on these established methods, we aim to develop a physics-informed neural network (PINN) for solving the NID-based inverse problem introduced in § 1.2.

A PINN is a neural network that solves forward and inverse problems while respecting the governing equations in the form of partial differential equations (PDEs) (Lagaris, Likas & Fotiadis 1998; Karniadakis *et al.* 2021). By reason of their ability to provide desirable solutions to ill-posed problems, PINNs have been used widely for the inverse modelling of dynamical systems. For example, Chen *et al.* (2020) employed a PINN to tackle ill-posed inverse scattering problems in nano-optics photonic metamaterials. Jagtap *et al.* (2022) used the extended PINN framework for addressing inverse supersonic compressible flow problems. For enhancing the training accuracy through inductive bias, hard-constrained PINNs for inverse problems are proposed in Lu *et al.* (2021). Recently, Ozan & Magri (2023) integrated a hard-constrained PINN and the Galerkin decomposition technique to model nonlinear acoustics in a prototypical thermoacoustic system. One can find further

theoretical foundations for the PINN approach to inverse problems in Mishra & Molinaro (2022) and Zhang, Li & Liu (2023).

In order to model the noise-induced behaviour of the thermoacoustic system, it is essential to incorporate SDEs into the PINN framework. Although not applied to thermoacoustic systems, recent studies have suggested that PINNs can be adopted to solve inverse problems of the SDEs (Xu & Darve 2021; Shin & Choi 2023), opening up possibilities for system identification in noise-perturbed combustors. However, only a limited number of studies have integrated stochastic samples with averaged PDEs, which is essential for system identification using the NID. For instance, Chen *et al.* (2021) proposed a PINN approach for solving inverse problems involving NID through the Fokker–Planck equation using discrete particle observations. The authors employed the Kullback–Leibler divergence from the observed empirical distribution to the neural network solution as a loss function. We, on the other hand, seek to minimize the discrepancy between the discrete samples and the analytical Fokker–Planck equation using the maximum likelihood approach, aiming to obtain more stable solutions suitable for system identification in noisy combustors.

1.4. *Contributions of the present study*

In this paper, we aim to develop and validate an NID-based system identification method that does not require the computation of the time correlation of the signal, and thus does not suffer from the discrete approximation error and the finite-time effect. Specifically, we aim to exploit a PINN linking the combustor signal and the Fokker–Planck equation equivalent to the stochastic Van der Pol equation for solving the inverse problem (i.e. system identification). A key mathematical distinction in our framework is the use of the maximum likelihood approach to integrate discrete samples with the Fokker–Planck equation, directly incorporating stochastic samples from the original SDE.

Below, we present our mathematical framework in § 2, focusing on the system model and PINN design. Next, we describe the numerical and experimental data for validating the proposed method in § 3. We then show the system identification results and the following discussion in § 4, before concluding in § 5.

2. Mathematical framework

2.1. *Stochastic self-sustained oscillator model*

Here, we describe briefly our system model and the corresponding probabilistic solution. One may refer to Lee *et al.* (2023*b*) for a more detailed mathematical description. First, we introduce a phenomenological low-order model for a thermoacoustically oscillating system. Specifically, we consider an SDE consisting of a Van der Pol type self-sustained oscillator equation and an additive noise term:

$$\frac{\mathrm{d}^2x}{\mathrm{d}t^2} - (\epsilon + \alpha x^2)\frac{\mathrm{d}x}{\mathrm{d}t} + \omega^2 x = \sqrt{2d}\,\eta, \quad \text{for } t > 0, \tag{2.1}$$

where x is the system variable (e.g. pressure in a combustor), η is a unit white Gaussian noise, and $d > 0$ is the amplitude of the noise. Here, ϵ and α are linear and nonlinear parameters, equivalent to k_1 and k_2 in (1.1), respectively, with scale factors. Finally, ω is the angular frequency of the oscillation that can be obtained easily from spectral analysis in practice. A probabilistic solution of (2.1) in the form of the Fokker–Planck equation can be obtained by applying the method of variation of parameters. Specifically, we transform

the system variable x and its derivative $\mathrm{d}x/\mathrm{d}t$ into the functions of amplitude (a) and phase (ϕ):

$$\left.\begin{aligned} x &= a\cos(\omega t+\phi),\\ \frac{\mathrm{d}x}{\mathrm{d}t} &= -a\omega\sin(\omega t+\phi). \end{aligned}\right\} \tag{2.2}$$

The method of variation of parameters shown above is used frequently for the analysis of stochastic nonlinear oscillators (Nayfeh 1981; Zhu & Yu 1987). By applying trigonometric identities, a set of SDEs is obtained:

$$\left.\begin{aligned} \frac{\mathrm{d}a}{\mathrm{d}t} &= \frac{\epsilon}{2}a+\frac{\alpha}{8}a^3+Q_1-\left(\frac{\sqrt{2d}}{\omega}\sin\Phi\right)\eta_1,\\ \frac{\mathrm{d}\phi}{\mathrm{d}t} &= Q_2-\left(\frac{\sqrt{2d}}{\omega a}\cos\Phi\right)\eta_2, \end{aligned}\right\} \tag{2.3}$$

where Φ is $\omega t+\phi(t)$, and Q_1 and Q_2 are the sums of first-order terms that become zero upon time averaging. Here, η_1 and η_2 are unit white Gaussian noise terms for amplitude and phase, respectively, each of which is an independent stochastic process with a correlation time smaller than the acoustic period (Bonciolini *et al.* 2021; Indlekofer *et al.* 2022). Therefore, we can confirm the equivalence of (2.1), (2.3) and (1.1) for zero noise ($d=0$) when averaged over sufficient time. Applying the stochastic averaging under the assumption of weak nonlinearity, we obtain the Fokker–Planck equation:

$$\left.\begin{aligned} \partial_t P(a,t) &= -\partial_a(D^{(1)}(a)\,P(a,t))+\partial_{aa}(D^{(2)}P(a,t)), \quad \text{for } (a,t)\in(0,\infty]\times[0,\infty],\\ P(a,0) &= P_0(a), \quad \text{for } a\in[0,\infty],\\ P(0,t) &= 0, \quad \text{for } t\in[0,\infty], \end{aligned}\right\} \tag{2.4}$$

where $D^{(1)}(a)=(\epsilon/2)a+(\alpha/8)a^3+d/2\omega^2 a$ and $D^{(2)}(a)=d/2\omega^2$.

2.2. *A PINN for solving the inverse problem*

In the system identification of thermoacoustic oscillators, we aim to determine the unknown system parameters ϵ, α and d in the SDE (2.1) from the discrete stochastic samples $\{x_{t_j}^{(i)}\}_{i=1}^{N}$ at various times t_j for $j=1,2,\ldots,M$. Although recent studies (Chen *et al.* 2021; Xu & Darve 2021; Shin & Choi 2023) have demonstrated successfully data-driven methods for solving such SDE-related inverse problems, training neural networks while adhering to SDE constraints typically demands a considerable number of samples, and may lead to unstable training. In our approach, we tackle these challenges by adopting deterministic surrogate modelling, specifically by integrating a smooth initial condition and domain truncation derived from the Fokker–Planck equation (Son & Lee 2023). The surrogate equation for a PINN-based system identification is

$$\left.\begin{aligned} \partial_t P(a,t) &= -\partial_a(D^{(1)}(a)\,P(a,t))+D^{(2)}\partial_{aa}P(a,t), \quad \text{for } (a,t)\in[0,A]\times[0,T],\\ P(a,0) &= \hat{P}(a), \quad \text{for } a\in[0,A],\\ P(0,t) &= 0, \quad \text{for } t\in[0,T], \end{aligned}\right\} \tag{2.5}$$

where $D^{(1)}(a)$ and $D^{(2)}(a)$ are as in § 2.1, and $\hat{P}(a)$ is a gamma distribution $\Gamma(\theta_1, \theta_2)$ with $\theta_1 \geq 2$ and $\theta_2 \gg 1$.

We aim to approximate simultaneously the solution of (2.5) and the unknown model parameters based on (2.5) with the stochastic samples $\{x_{t_j}^{(i)}\}_{i=1}^N$. To achieve this, we utilize a fully connected neural network to approximate the solution, and three additional learnable parameters ϵ, α and d to approximate the unknown model parameters. The network comprises three hidden layers, each composed of 64 hidden units activated by the hyperbolic tangent function. The output layer is fed to the softplus function $F(x) = \log(1 + \mathrm{e}^x)$, ensuring that the network output remains non-negative. We define three loss functions: $\mathcal{L}_R$ for the PDE residual, $\mathcal{L}_{BC}$ for the boundary condition, and $\mathcal{L}_{mass}$ to ensure that the solution conforms to the properties of a probability density function (p.d.f.). Mathematically, these functions are represented as

$$\left.\begin{aligned} \mathcal{L}_R &= \|\partial_t P(a,t) + \partial_a(D^{(1)}(a)\,P(a,t)) - D^{(2)}\partial_{aa}P(a,t)\|^2_{L^2([0,A]\times[0,T])}, \\ \mathcal{L}_{BC} &= \|P(a,t)\|^2_{L^2(\{0\}\times[0,T])}, \\ \mathcal{L}_{mass} &= \left\| \int_{[0,A]} P(a,t)\,\mathrm{d}a - 1 \right\|^2_{L^2([0,T])}, \end{aligned}\right\} \tag{2.6}$$

where the learnable parameters ϵ, α and d contribute to $\mathcal{L}_R$ through $D^{(1)}(a)$ and $D^{(2)}$. Note that we excluded the surrogate initial condition from the loss function, as the initial data will be given repeatedly in stochastic samples.

System identification of (2.5) requires integrating the stochastic samples $\{x_{t_j}^{(i)}\}_{i=1}^N$ with the solution of the Fokker–Planck equation (2.5), which represents the p.d.f. of the amplitude variable a at time t. Our process begins by transforming the samples $\{x_{t_j}^{(i)}\}_{i=1}^N$ into amplitudes $\{a_{t_j}^{(i)}\}_{i=1}^N$ through the use of the Hilbert transform. To facilitate the integration, we make an independence assumption about the samples $\{x_{t_j}^{(i)}\}_{i=1}^N$ for each time t_j for $j = 1, \ldots, M$. This assumption allows us to incorporate the concept of maximum likelihood estimation into the loss function of PINN. Because maximizing likelihood is equivalent to minimizing negative log-likelihood, we define a data loss function by the sum of negative log-likelihood as

$$\mathcal{L}_{data} = \sum_{j=1}^{N} -\log\left(\prod_{i=1}^{N} P(a_i, t_j)\right) = -\sum_{i,j=1}^{N,M} \log P(a_i, t_j). \tag{2.7}$$

Finally, we solve an optimization problem:

$$\min_{W,\epsilon,\alpha,d} \lambda_1\mathcal{L}_R + \lambda_2\mathcal{L}_{BC} + \lambda_3\mathcal{L}_{mass} + \lambda_4\mathcal{L}_{data}, \tag{2.8}$$

for some $\lambda_1, \lambda_2, \lambda_3, \lambda_4$, where W denotes the network parameters. Adam optimizer (Kingma & Ba 2014) is used for the optimization. The overall architecture of the proposed PINN-based system identification is illustrated in figure 1.

3. Data for PINN validation

3.1. *Synthetic data*

For the validation of the PINN-based system identification framework, we use both the synthetic data and the experimental data. First, we consider six sets of synthetic data,

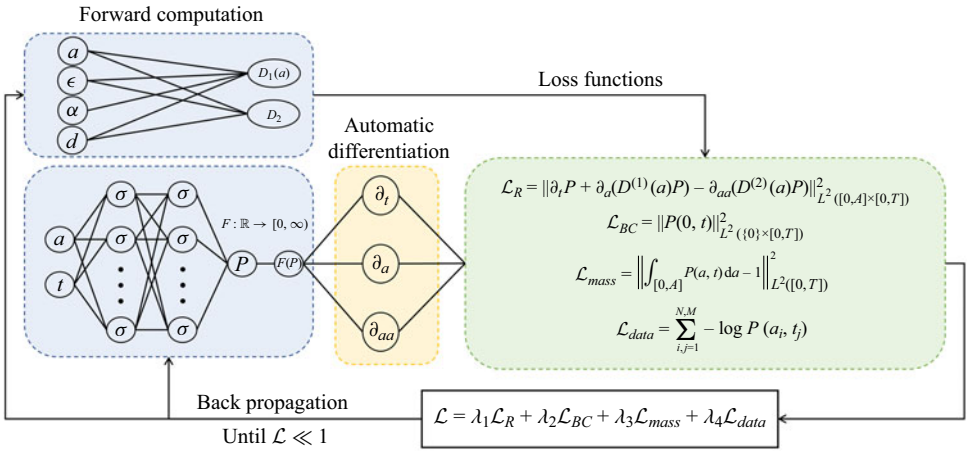

Figure 1. The architecture of the PINN designed for identifying the parameters of the self-sustained thermoacoustic oscillator. We utilize a fully connected neural network providing non-negative output value, and three additional learnable parameters ϵ, α and d. Network output is processed through automatic differentiation and combined with ϵ, α and d to compute the loss functions as defined in (2.6) and (2.7). We update both the network parameters and the additional learnable parameters through back propagation until convergence is achieved.

each containing ten numerically generated time series. These time series feature stochastic transient self-sustained oscillation displayed in figures 2(*a–f*). Three sets of data are in the fixed-point regime before the Hopf bifurcation ($\epsilon = -0.3, -0.2, -0.1$), while the other three sets are in the limit-cycle regime after the Hopf point ($\epsilon = +0.1, +0.2, +0.3$). Other system parameters are are set as $\alpha = -0.1$, $d = 0.1$ and $\omega = 2\pi$, as per Son & Lee (2023).

Synthetic data are created by solving (2.1) numerically with the fourth-order Runge–Kutta method for $t = [0, 100]$ with $\mathrm{d}t = 0.01$. When solving the time-marching problem, We set the initial values of $[x, \mathrm{d}x/\mathrm{d}t]$ as $[1, 0]$ for fixed-point data, and $[0, 0]$ for limit-cycle data. These initial conditions enable the observation of transient amplitude death in the fixed-point regime and amplitude growth in the limit-cycle regime, as depicted in figures 2(*a–l*). Time evolution of the oscillation amplitudes computed from the Hilbert transform are shown collectively in figures 2(*g–l*), while their p.d.f.s are shown in figures 2(*m–r*). The saturation in deterministic oscillation amplitude is found at $t > 80$ for all synthetic data, indicating zero-amplitude fixed points with stochastic fluctuation ($\epsilon < 0$) and fully developed self-sustained oscillations ($\epsilon > 0$). It is worth noting that the amplitude saturation is slower in the weakly nonlinear time series where the absolute value of the linear growth rate is close to zero.

3.2. *Experimental data*

As for the experimental validation, we use the pressure data obtained from an annular model gas-turbine combustor identical to that in Guk *et al.* (2023) (figure 3*a*). In this set-up, gaseous methane (purity 95.95 %) is premixed with air, which is passed through the dryer (Kyungwon T15K) and compressor (Kyungwon AL5N), before entering the combustor via a swirler and a nozzle. The swirler and the nozzle, respectively, have swirl number 0.608 and diameter 35 mm. The annular combustor has inner diameter 395 mm and outer diameter 405 mm, and is manufactured with SUS304 stainless steel except for the inner wall. A cylindrical quartz serves as the inner wall of the annular combustor, enabling the visual inspection of the flame via two planar mirrors. Nine circular openings with diameter 60 mm are installed at the combustor ceiling, which constitutes the flow exit

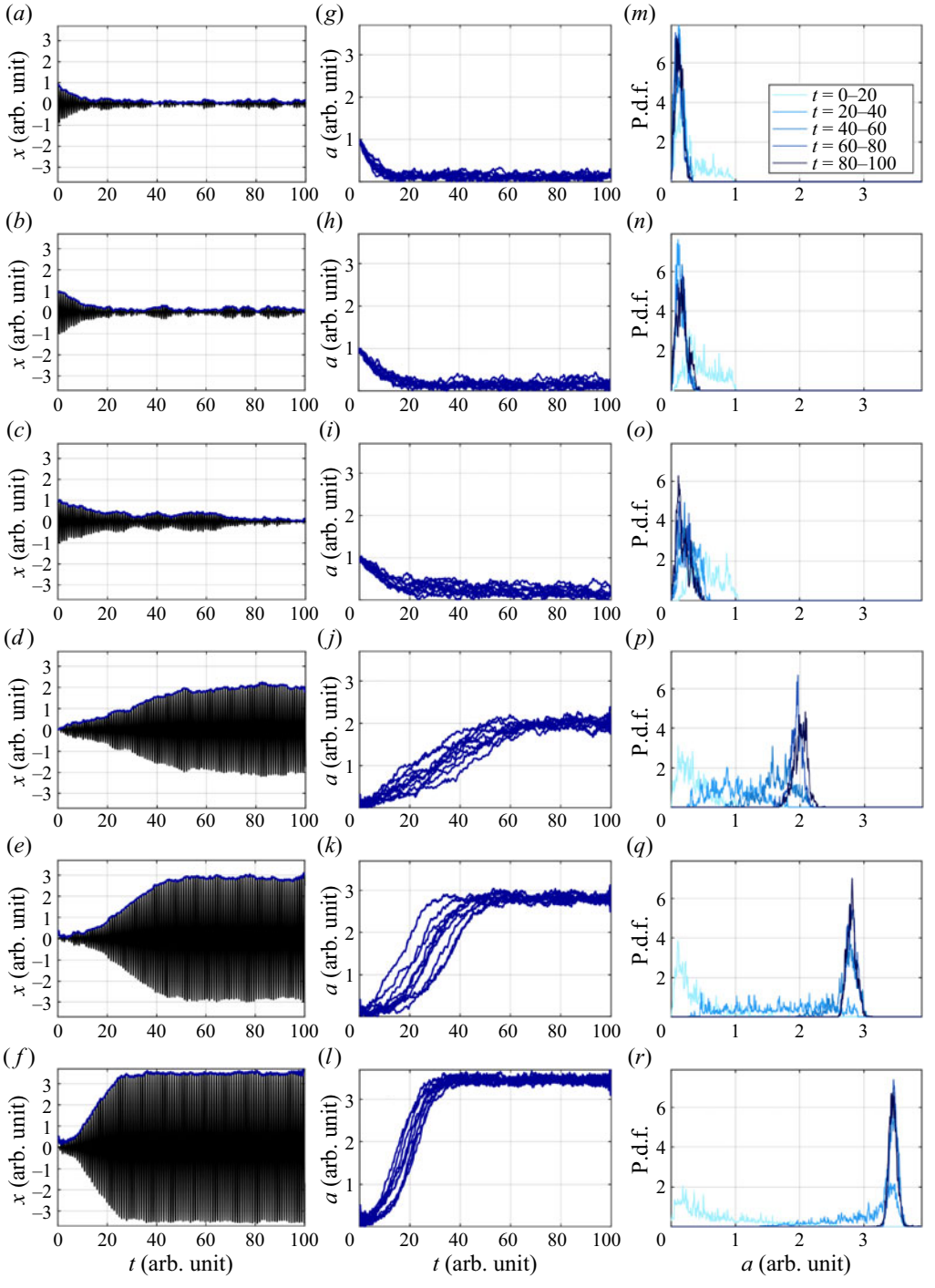

Figure 2. (*a–f*) Sample time series (black line) and the amplitude (blue line) used for PINN training. (*g–l*) Time evolution of the amplitude in ten sample time series at each case, and (*m–r*) their p.d.f.s. Six sets of synthetic data are displayed: $(a,g,m)\ \epsilon = -0.3$, $(b,h,n)\ \epsilon = -0.2$, $(c,i,o)\ \epsilon = -0.1$ at the fixed-point regime, and $(d,j,p)\ \epsilon = +0.1$, $(e,k,q)\ \epsilon = +0.2$, $(f,l,r)\ \epsilon = +0.3$ at the limit-cycle regime. Here, α, d and ω are fixed at -0.1, 0.1 and 2π in all cases.

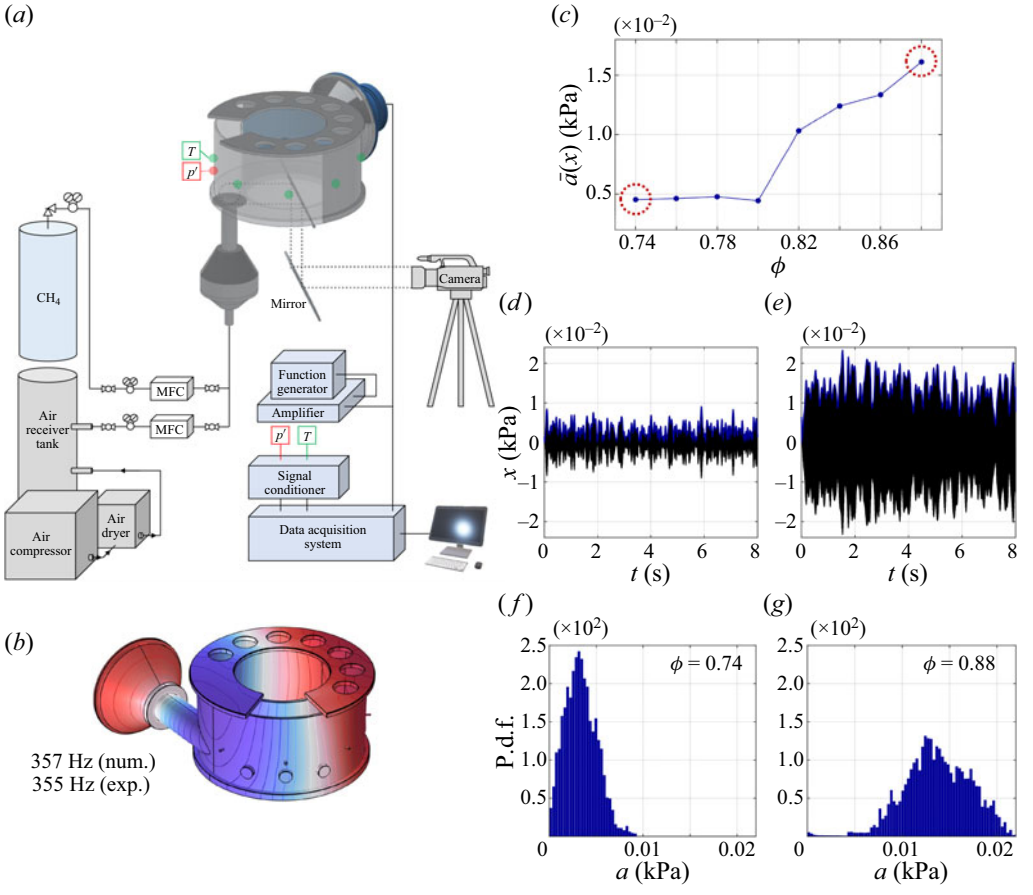

Figure 3. (*a*) Schematic diagram of the annular combustor identical to that in Guk, Seo & Lee (2023). (*b*) Mode of interest featuring transverse acoustic oscillation, and (*c*) mean oscillation amplitude of this mode at varying methane–air equivalence ratio (ϕ). (*d*,*e*) Bandpass-filtered pressure signal (black line) and its amplitude (blue line), and (*f*,*g*) p.d.f.s of the amplitude at (*d*,*f*) the fixed-point regime ($\phi = 0.74$) and (*e*,*g*) the limit-cycle regime ($\phi = 0.88$). MFC: mass flow controller.

along with a fan-shaped opening at the top of the nozzle. The methane–air equivalence ratio is varied between 0.74 (lean blowoff limit) and 0.9, with step size 0.02, while the total mass flow rate is kept to 5.5 g s^{-1} via mass flow controllers (MKP TSC-230 and MKP TSC-145 for fuel and air, respectively). Pressure oscillation in the combustor is measured with a piezoelectric transducer (PCB 113B28) installed 50 mm above the nozzle exit. At each equivalence ratio condition, the combustion experiment is conducted for 8 s. The pressure signal is recorded with sampling rate 25 000 Hz, which is much faster than the mode of interest described below.

By inspecting the oscillatory dynamics of the pressure signal, we found a distinct transverse mode at 355 Hz, which matches the result of the acoustic numerical simulation (figure 3(*b*), simulated using COMSOL Multiphysics v6.1). At this mode, a gradual increase in pressure oscillation amplitude is observed (figure 3*c*), implying a weakly nonlinear oscillation near a supercritical Hopf bifurcation. For diagnosing the thermoacoustic system both before and after the Hopf bifurcation, we select two experimental conditions, one in the fixed-point regime ($\phi = 0.74$) and the other in the limit-cycle regime ($\phi = 0.88$). The pressure time series and p.d.f.s of the oscillation

amplitude at these conditions are shown in figures 3(*d–g*). Although the system identification using the stochastic Van der Pol equation (2.1) and the corresponding Fokker–Planck equation (2.4) often requires external stochastic forcing for inducing the NID (Lee *et al.* 2019, 2020), we do not excite the system with additional noise, recognizing the strong inherent turbulence within the combustor (Noiray & Schuermans 2013; Lee *et al.* 2021).

We employed time segmentation for the experimental data, which significantly improves training stability by increasing the number of samples at each time point. To be more precise, we partitioned each experimental dataset into eight time segments, assuming that the data are collected at the initial time point of each segment, i.e. $t = 0, 1, \ldots, 7$. This assumption is substantiated by the fact that all experimental data originated from the stationary regime. It is worth mentioning that we have used an identical network for both the synthetic and experimental validations, differing only in the dataset used to train the log-likelihood loss function. In other words, we employed identical initial networks and maintained consistent loss functions, adjusting only the data for each specific problem.

4. Results and discussion

In this section, we assess the results of PINN-based system identification in terms of the parameter accuracy and the likelihood of the reconstructed p.d.f. We also present comparisons of the results to the existing methods of system identification that use the NID, which use extrapolation of the time correlation (Lade 2009; Noiray & Schuermans 2013), and the same method with adjoint-based optimization (Boujo & Noiray 2017). These methods will be denoted SI-ext and SI-opt, respectively, in the following figures. In both of the established methods, drift and diffusion terms are estimated using the equation

$$D^{(n)}(a) = \lim_{\tau \to 0} D_\tau^{(n)}(a), \tag{4.1}$$

where $D_\tau^{(n)}(a)$ is defined by

$$D_\tau^{(n)}(a) = \frac{1}{n!\,\tau} \int_0^\infty (A - a)^n \, P(A, t + \tau \mid a, t) \, \mathrm{d}A, \tag{4.2}$$

where $P(A, t + \tau \mid a, t)$ is the conditional p.d.f. of the pressure oscillation amplitude being A at time $t + \tau$ given a at time t. In the adjoint-based optimization framework (SI-opt), the discrepancy between $D_\tau^{(n)}(a)$ computed from the obtained parameters and the experimental measurement is minimized using the optimization scheme (Boujo & Noiray 2017). It should be noted that neither the time-shifted drift/diffusion term estimation nor the adjoint-based optimization is applied in the proposed PINN framework, and these methods are used only for comparing the extracted system parameters in this paper. For further information about these existing methods, readers may refer to Lee *et al.* (2023*b*).

First, for identifying the governing parameters of the synthetic limit-cycle data, we initialized ϵ, α and d to be zero and applied the Xavier initialization for the network parameters before training, following the guidelines outlined by Glorot & Bengio (2010). For the computation of loss functions $\mathcal{L}_R$ and $\mathcal{L}_{mass}$, we sampled 10 000 collocation points from the domain $[0, A] \times [0, T]$. Additionally, we sampled 100 points for each component of $\mathcal{L}_{BC}$. We set the initial learning rate at 10^{-4}, and reduced it systematically using a learning rate scheduler throughout the training process.

Figures 4(*a–f*) show the evolution of the parameters as training iterates when using synthetic transient data. While the parameters ϵ, α, d converge rapidly in the limit-cycle

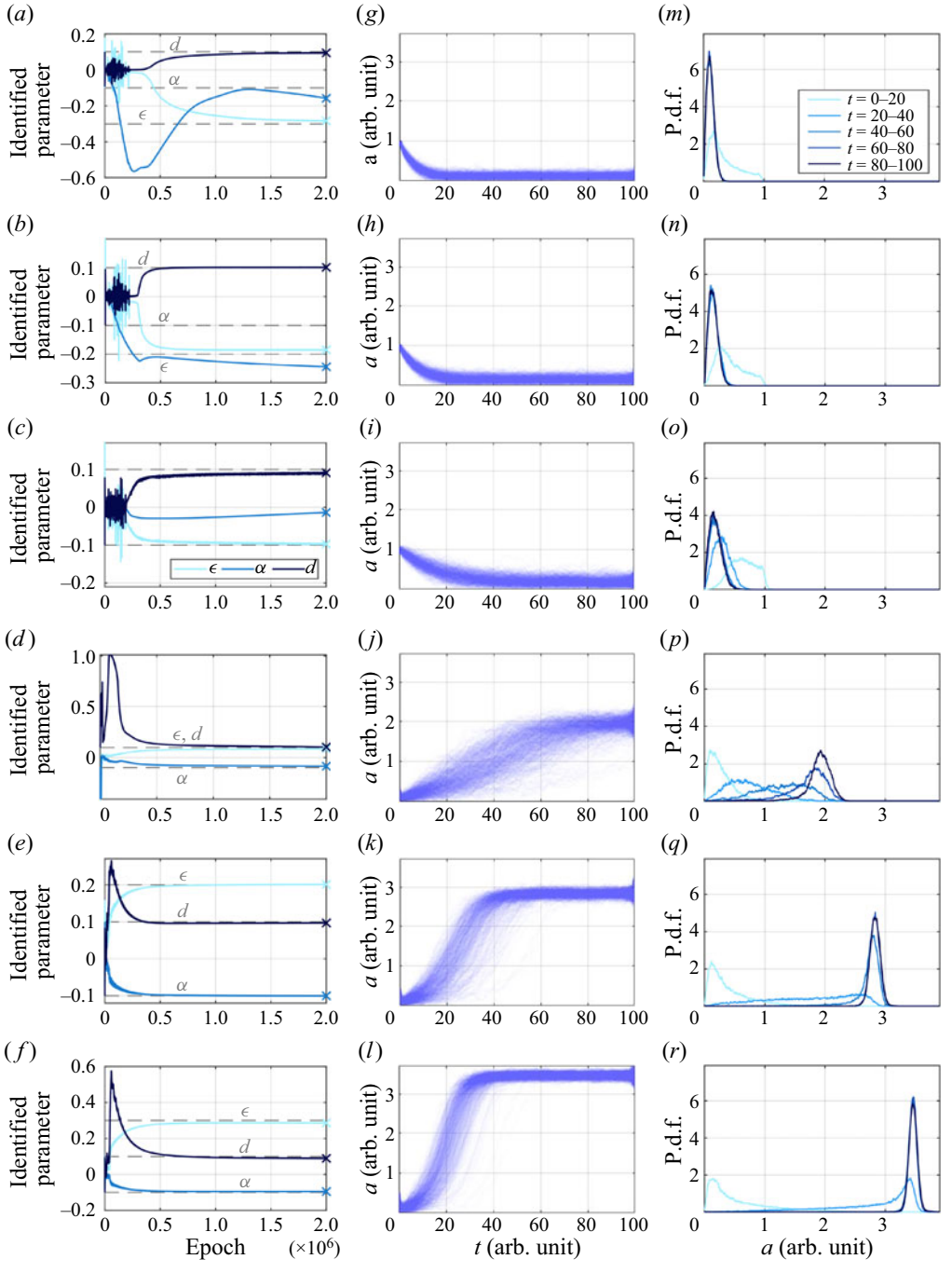

Figure 4. (*a–f*) The convergence history of ϵ, α, d during PINN-based system identification. (*g–l*) Time evolution of the oscillation amplitude obtained from 500 numerical repetitions using the identified parameters, and (*m–r*) the corresponding p.d.f.s. The results are obtained from six sets of synthetic data: (*a*,*g*,*m*) $\epsilon = -0.3$, (*b*,*h*,*n*) $\epsilon = -0.2$, (*c*,*i*,*o*) $\epsilon = -0.1$ at the fixed-point regime, and (*d*,*j*,*p*) $\epsilon = +0.1$, (*e*,*k*,*q*) $\epsilon = +0.2$, (*f*,*l*,*r*) $\epsilon = +0.3$ at the limit-cycle regime. Here, α, d and ω are fixed at -0.1, 0.1 and 2π in all cases. Grey dashed lines indicate true values of ϵ, α and d.

		SI-ext	SI-opt	PINN	True			SI-ext	SI-opt	PINN	True
$\epsilon = -0.1$	ϵ	−0.182	−0.120	−0.097	−0.1	$\epsilon = 0.1$	ϵ	0.113	0.101	0.087	0.1
	α	0.138	−0.016	−0.014	−0.1		α	−0.107	−0.097	−0.086	−0.1
	d	0.125	0.091	0.091	0.1		d	0.222	0.054	0.105	0.1
	E	115 %	38 %	33 %	—		E	47 %	17 %	10.8 %	—
$\epsilon = -0.2$	ϵ	−0.328	−0.208	−0.185	−0.2	$\epsilon = 0.2$	ϵ	0.217	0.217	0.201	0.2
	α	0.467	−0.305	−0.245	−0.1		α	−0.111	−0.109	−0.100	−0.1
	d	0.131	0.108	0.102	0.1		d	1.278	0.059	0.097	0.1
	E	221 %	73 %	51 %	—		E	399 %	19 %	1.2 %	—
$\epsilon = -0.3$	ϵ	−0.463	−0.309	−0.284	−0.3	$\epsilon = 0.3$	ϵ	0.270	0.297	0.286	0.3
	α	0.462	−0.331	−0.158	−0.1		α	−0.093	−0.099	−0.096	−0.1
	d	0.135	0.092	0.094	0.1		d	3.600	0.081	0.089	0.1
	E	217 %	81 %	23 %	—		E	1172 %	7.0 %	6.6 %	—

Table 1. Parameters identified from synthetic data using the following methods: extrapolation-based system identification (SI-ext), adjoint-optimization-based system identification (SI-opt) and PINN. Here, E is the average relative error of the identified parameters (ϵ, α, d) compared to true values.

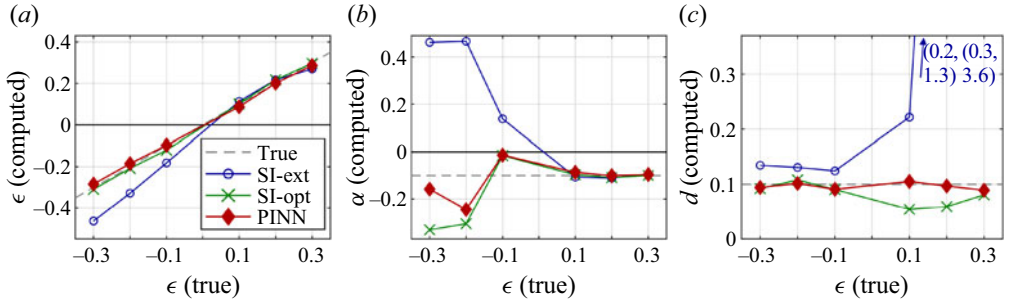

Figure 5. Parameters of the stochastic Van der Pol equation computed from extrapolation-based system identification (SI-ext, blue line with circular markers), system identification with adjoint-based optimization (SI-opt, green line with cross markers), and the present method (PINN, red line with diamond markers).

cases ($\epsilon > 0$), fixed-point cases ($\epsilon < 0$) tend to require greater number of iterations for convergence, especially when the system deviates further from the Hopf point ($\epsilon = 0$). This is because the fixed-point data are generally less deterministic compared to limit-cycle counterparts, and thus have a wider choice of system parameters for minimizing the loss function. Such a trend is also found in existing system identification methods, as shown in table 1. Nevertheless, in all cases, PINN-based system identification shows substantial improvement from the existing system identification methods in terms of the average relative error of the identified parameters (see table 1). As a result, we were able to reconstruct accurately the time evolution of the oscillation amplitude and its corresponding p.d.f. for both the fixed-point and limit-cycle data, as shown in figures 4(g–r). Considering that just ten stochastic signals (figure 2) are used as the input data in each case, the accuracy of the present system identification framework is recognizable. Again, the parameters identified from the PINN approach are closer to the true values in all test cases, as depicted in figure 5.

Next, we present the PINN-based system identification results for the annular combustor data in table 2 and figure 6. Because the true values of the governing parameters of the thermoacoustic oscillation are unknown, we alternatively assess the average likelihood values $L_{avg} = -(1/M)\sum_{i,j=1}^{N,M} \log P(a_i, t_j)$ of the analytical solution computed from the identified parameters. It can be seen from table 2 that L_{avg} is greatest in the PINN-based

	(*a*)			(*b*)		
	SI-ext	SI-opt	PINN	SI-ext	SI-opt	PINN
ϵ	-3.53	-6.61	-1.40×10	1.75	1.07×10	4.74
α	7.61×10^4	-7.84×10^5	-7.40×10^5	-6.28×10^4	-2.14×10^5	-9.94×10^4
d	1.21×10^2	3.34×10^2	6.67×10^2	5.73×10^2	7.59×10^2	6.52×10^2
L_{avg}	4.98	5.00	5.02	4.07	4.13	4.18

Table 2. Parameters identified from experimental data at the equivalence ratios (*a*) $\phi = 0.74$ and (*b*) $\phi = 0.88$, using the following methods: extrapolation-based system identification (SI-ext), adjoint-optimization-based system identification (SI-opt) and PINN. Here, L_{avg} is the likelihood of the p.d.f. reconstructed from identified parameters ϵ, α, d.

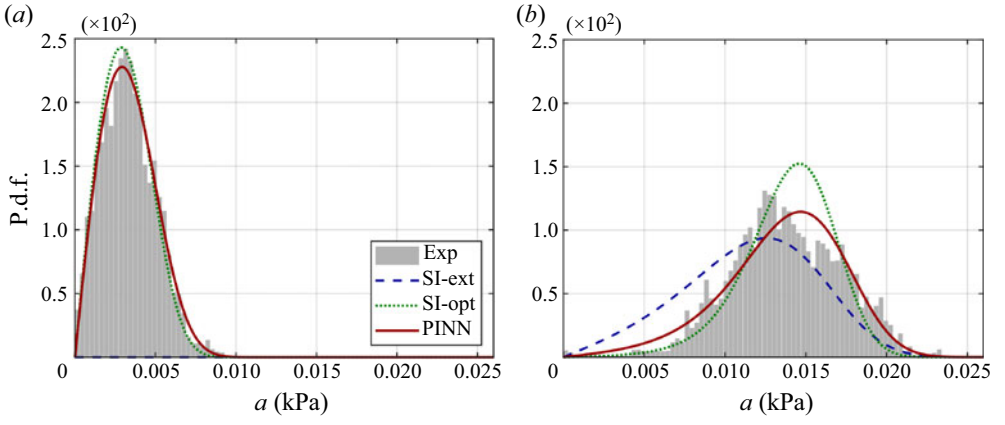

Figure 6. Comparison between the experimental data (grey bars) and stationary analytical Fokker–Planck solutions using parameters computed from extrapolation-based system identification (SI-ext, blue dashed line), system identification with adjoint-based optimization (SI-opt, green dotted line), and the present method (PINN, red continuous line) at (*a*) the fixed-point regime ($\phi = 0.74$) and (*b*) the limit-cycle regime ($\phi = 0.88$). The stationary analytical solution could not be computed with SI-ext parameters at $\phi = 0.74$ because of the diverging solution ($\alpha > 0$). Here, ϕ is the methane–air equivalence ratio.

system identification for both the fixed-point and limit-cycle data. This indicates that the parameters computed from the PINN approach best represent the experimental p.d.f., especially in the limit-cycle regime (see figure 6 for comparison).

Finally, we reconstruct the phase portrait of the limit cycle from the computed parameters of thermoacoustic oscillation. We use the delay embedding technique proposed by Takens (1981), which enables the reconstruction of the phase portrait using just a single time series with a time delay (τ). This method is used widely to examine the dynamics of thermoacoustic oscillations (Kashinath, Li & Juniper 2018; Lee *et al.* 2020). Following Fraser & Swinney (1986), we choose the minimum τ that minimizes the average mutual information. The reconstructed phase portraits shown in figure 7 reveal that the parameters identified from the PINN-based framework best capture the dynamics of the experimental data in both the fixed-point and limit-cycle regimes, reconfirming the robustness of the present method.

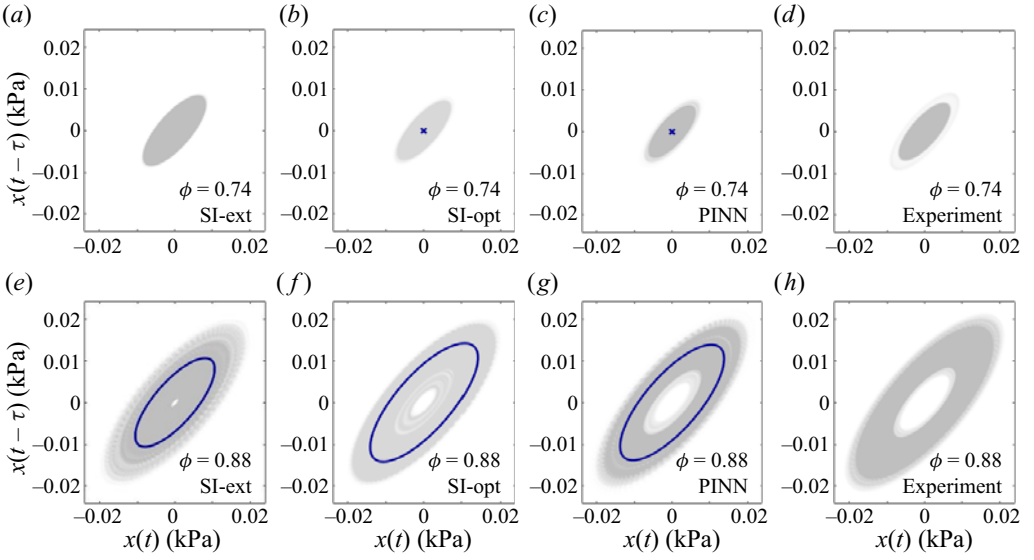

Figure 7. Phase portraits obtained from (*a–c*,*e–g*) numerical simulations and (*d*,*h*) experimental data. Numerical results are computed using the system identification results of the experimental data obtained from (*a*,*e*) extrapolation-based SI (SI-ext), (*b*,*f*) SI with adjoint-based optimization (SI-opt), and (*c*,*g*) the present method (PINN). Grey scatter dots are obtained from the stochastic signal, while blue lines are computed from deterministic ($d = 0$) simulations. Cross markers in (*b*,*c*) indicate analytical fixed points, while the fixed point could not be obtained with SI-ext parameters at $\phi = 0.74$ because of the diverging solution ($\alpha > 0$). Here, τ is the time delay computed from the minimum average mutual information (Fraser & Swinney 1986), and ϕ is the methane–air equivalence ratio.

5. Conclusions

In this study, we performed NID-based system identification of a thermoacoustic oscillator in fixed-point and limit-cycle regimes using the PINN approach. From numerical and experimental validation, we found that the system identification using PINN leads to better computation performance than existing system identification methods that incorporate NID, in terms of parameter accuracy and likelihood. This is the first time that PINN has been applied for diagnosing thermoacoustic oscillations modelled with a stochastic oscillator equation, to the best of our knowledge. A major implication of this study is that the proposed framework could identify accurately the parameters of the stochastic self-sustained oscillation using the output-only method without requiring information about the input signal or the adjoint-based optimization schemes. Thus an efficient and versatile system identification could be performed in a noisy thermoacoustic system by capturing the NID from the PINN framework.

There are three categories of studies that can be explored in the future. First, albeit not demonstrated in this paper, parameters of the stochastic Van der Pol equation identified from the present framework can be used to predict and control the thermoacoustic instabilities. Specifically, the Hopf point and the post-bifurcation dynamics can be predicted via the extrapolation of the identified parameters (Lee *et al.* 2020), and the feedback control can be conducted using these parameters. Second, the present study dealt with the occurrence of thermoacoustic oscillation via the supercritical Hopf bifurcation. In future research, other routes to instabilities involving higher-order dynamics, such as subcritical Hopf bifurcation (Gopalakrishnan *et al.* 2016), intermittency (Nair, Thampi & Sujith 2014) and period doubling (Subramanian *et al.* 2010), can be studied using

the present PINN-based method. Finally, considering that the system model used in this study is purely phenomenological, the present framework can be applied to other physical systems exhibiting stochastic self-sustained oscillations. For example, one can apply PINN-based system identification to diagnose hydrodynamically oscillating low-density jets (Zhu, Gupta & Li 2017; Lee *et al.* 2019; Park & Lee 2024) or electrically oscillating plasma in Hall-effect thrusters (Han *et al.* 2023; Lee *et al.* 2023*a*).

Funding. This work was supported by a National Research Foundation of Korea (NRF) grant funded by the Korea government (MSIT) (no. NRF-2022R1F1A1073732).

Declaration of interests. The authors report no conflict of interest.

Author ORCIDs.
Hwijae Son https://orcid.org/0000-0002-6630-2832;
Minwoo Lee https://orcid.org/0000-0002-1025-0260.

References

Bonciolini, G., Boujo, E. & Noiray, N. 2017 Output-only parameter identification of a colored-noise-driven Van-der-Pol oscillator: thermoacoustic instabilities as an example. *Phys. Rev.* E **95** (6), 062217.

Bonciolini, G., Faure-Beaulieu, A., Bourquard, C. & Noiray, N. 2021 Low order modelling of thermoacoustic instabilities and intermittency: flame response delay and nonlinearity. *Combust. Flame* **226**, 396–411.

Boujo, E. & Noiray, N. 2017 Robust identification of harmonic oscillator parameters using the adjoint Fokker–Planck equation. *Proc. R. Soc. Lond.* A **473** (2200), 20160894.

Chen, X., Yang, L., Duan, J. & Karniadakis, G.E. 2021 Solving inverse stochastic problems from discrete particle observations using the Fokker–Planck equation and physics-informed neural networks. *SIAM J. Sci. Comput.* **43** (3), B811–B830.

Chen, Y., Lu, L., Karniadakis, G.E. & Dal Negro, L. 2020 Physics-informed neural networks for inverse problems in nano-optics and metamaterials. *Opt. Express* **28** (8), 11618–11633.

Fraser, A.M. & Swinney, H.L. 1986 Independent coordinates for strange attractors from mutual information. *Phys. Rev.* A **33** (2), 1134.

Glorot, X. & Bengio, Y. 2010 Understanding the difficulty of training deep feedforward neural networks. In *Proceedings of the Thirteenth International Conference on Artificial Intelligence and Statistics*, pp. 249–256. JMLR Workshop and Conference Proceedings.

Gopalakrishnan, E.A., Sharma, Y., John, T., Dutta, P.S. & Sujith, R.I. 2016 Early warning signals for critical transitions in a thermoacoustic system. *Sci. Rep.* **6** (1), 35310.

Guk, S., Seo, S. & Lee, M. 2023 Thermoacoustic dynamics in an annular model gas-turbine combustor under transverse stochastic forcing. *J. Korean Soc. Combust.* **28** (3), 20–27.

Han, E., Kim, D., Lee, J., Kim, Y., Yi, M. & Lee, M. 2023 Analysis of the Hall-effect thruster discharge instability using complexity-entropy causality plane. *J. Korean Soc. Aeronaut. Space Sci.* **51** (4), 263–271.

Indlekofer, T., Faure-Beaulieu, A., Dawson, J.R. & Noiray, N. 2022 Spontaneous and explicit symmetry breaking of thermoacoustic eigenmodes in imperfect annular geometries. *J. Fluid Mech.* **944**, A15.

Jaensch, S. & Polifke, W. 2017 Uncertainty encountered when modelling self-excited thermoacoustic oscillations with artificial neural networks. *Intl J. Spray Combust. Dyn.* **9** (4), 367–379.

Jagtap, A.D., Mao, Z., Adams, N. & Karniadakis, G.E. 2022 Physics-informed neural networks for inverse problems in supersonic flows. *J. Comput. Phys.* **466**, 111402.

Juniper, M.P. & Sujith, R.I. 2018 Sensitivity and nonlinearity of thermoacoustic oscillations. *Annu. Rev. Fluid Mech.* **50**, 661–689.

Kabiraj, L., Steinert, R., Saurabh, A. & Paschereit, C.O. 2015 Coherence resonance in a thermoacoustic system. *Phys. Rev.* E **92**, 042909.

Kabiraj, L., Vishnoi, N. & Saurabh, A. 2020 A review on noise-induced dynamics of thermoacoustic systems. In *Dynamics and Control of Energy Systems*, pp. 265–281. Springer.

Karniadakis, G.E., Kevrekidis, I.G., Lu, L., Perdikaris, P., Wang, S. & Yang, L. 2021 Physics-informed machine learning. *Nat. Rev. Phys.* **3** (6), 422–440.

KASHINATH, K., LI, L.K.B. & JUNIPER, M.P. 2018 Forced synchronization of periodic and aperiodic thermoacoustic oscillations: lock-in, bifurcations and open-loop control. *J. Fluid Mech.* **838**, 690–714.

KINGMA, D.P. & BA, J. 2014 Adam: a method for stochastic optimization. In *Proceedings of International Conference on Learning Representations, 2015*, pp. 1–15.

KRISHNAN, A., SUJITH, R.I., MARWAN, N. & KURTHS, J. 2021 Suppression of thermoacoustic instability by targeting the hubs of the turbulent networks in a bluff body stabilized combustor. *J. Fluid Mech.* **916**, A20.

LADE, S.J. 2009 Finite sampling interval effects in Kramers–Moyal analysis. *Phys. Lett.* A **373** (41), 3705–3709.

LAGARIS, I.E., LIKAS, A. & FOTIADIS, D.I. 1998 Artificial neural networks for solving ordinary and partial differential equations. *IEEE Trans. Neural Netw.* **9** (5), 987–1000.

LANDAU, L.D. 1944 On the problem of turbulence. *Dokl. Akad. Nauk SSSR* **44** (8), 339–349.

LEE, M., GUAN, Y., GUPTA, V. & LI, L.K.B. 2020 Input–output system identification of a thermoacoustic oscillator near a Hopf bifurcation using only fixed-point data. *Phys. Rev.* E **101** (1), 013102.

LEE, M., KIM, D., LEE, J., KIM, Y. & YI, M. 2023*a* A data-driven approach for analyzing Hall thruster discharge instability leading to plasma blowoff. *Acta Astronaut.* **206**, 1–8.

LEE, M., KIM, K.T., GUPTA, V. & LI, L.K.B. 2021 System identification and early warning detection of thermoacoustic oscillations in a turbulent combustor using its noise-induced dynamics. *Proc. Combust. Inst.* **38** (4), 6025–6033.

LEE, M., KIM, K.T. & PARK, J. 2023*b* A numerically efficient output-only system-identification framework for stochastically forced self-sustained oscillators. *Probab. Engng Mech.* **74**, 103516.

LEE, M., ZHU, Y., LI, L.K.B. & GUPTA, V. 2019 System identification of a low-density jet via its noise-induced dynamics. *J. Fluid Mech.* **862**, 200–215.

LIEUWEN, T. & YANG, V. 2005 *Combustion Instabilities in Gas Turbine Engines: Operational Experience, Fundamental Mechanisms and Modeling*. AIAA.

LU, L., PESTOURIE, R., YAO, W., WANG, Z., VERDUGO, F. & JOHNSON, S.G. 2021 Physics-informed neural networks with hard constraints for inverse design. *SIAM J. Sci. Comput.* **43** (6), B1105–B1132.

MAGRI, L., JUNIPER, M.P. & MOECK, J.P. 2020 Sensitivity of the Rayleigh criterion in thermoacoustics. *J. Fluid Mech.* **882**, R1.

MISHRA, S. & MOLINARO, R. 2022 Estimates on the generalization error of physics-informed neural networks for approximating a class of inverse problems for PDEs. *IMA J. Numer.* **42** (2), 981–1022.

NAIR, V., THAMPI, G. & SUJITH, R.I. 2014 Intermittency route to thermoacoustic instability in turbulent combustors. *J. Fluid Mech.* **756**, 470–487.

NAYFEH, A.H. 1981 *Introduction to Perturbation Techniques*. John Wiley.

NOIRAY, N. & DENISOV, A. 2017 A method to identify thermoacoustic growth rates in combustion chambers from dynamic pressure time series. *Proc. Combust. Inst.* **36** (3), 3843–3850.

NOIRAY, N. & SCHUERMANS, B. 2013 Deterministic quantities characterizing noise driven Hopf bifurcations in gas turbine combustors. *Intl J. Non-Linear Mech.* **50**, 152–163.

NÓVOA, A. & MAGRI, L. 2022 Real-time thermoacoustic data assimilation. *J. Fluid Mech.* **948**, A35.

NÓVOA, A., RACCA, A. & MAGRI, L. 2024 Inferring unknown unknowns: regularized bias-aware ensemble Kalman filter. *Comput. Meth. Appl. Mech. Engng* **418**, 116502.

OZAN, D.E. & MAGRI, L. 2023 Hard-constrained neural networks for modeling nonlinear acoustics. *Phys. Rev. Fluids* **8**, 103201.

PARK, S. & LEE, M. 2024 A semi-supervised framework for analyzing the potential core of a low-density jet. *Flow Meas. Instrum.* **95**, 102516.

PIKOVSKY, A.S. & KURTHS, J. 1997 Coherence resonance in a noise-driven excitable system. *Phys. Rev. Lett.* **78**, 775–778.

RAGHU, S. & MONKEWITZ, P.A. 1991 The bifurcation of a hot round jet to limit-cycle oscillations. *Phys. Fluids* A **3**, 501.

SELIMEFENDIGIL, F. & POLIFKE, W. 2011 A nonlinear frequency domain model for limit cycles in thermoacoustic systems with modal coupling. *Intl J. Spray Combust. Dyn.* **3** (4), 303–330.

SHIN, H. & CHOI, M. 2023 Physics-informed variational inference for uncertainty quantification of stochastic differential equations. *J. Comput. Phys.* **487**, 112183.

SIEGERT, S., FRIEDRICH, R. & PEINKE, J. 1998 Analysis of data sets of stochastic systems. *Phys. Lett.* A **243** (5–6), 275–280.

SON, H. & LEE, M. 2023 Continuous probabilistic solution to the transient self-oscillation under stochastic forcing: a PINN approach. *J. Mech. Sci. Technol.* **37** (8), 3911–3918.

STUART, J.T. 1960 On the non-linear mechanics of wave disturbances in stable and unstable parallel flows – part 1. The basic behaviour in plane Poiseuille flow. *J. Fluid Mech.* **9**, 353–370.

SUBRAMANIAN, P., MARIAPPAN, S., SUJITH, R.I. & WAHI, P. 2010 Bifurcation analysis of thermoacoustic instability in a horizontal Rijke tube. *Intl J. Spray Combust. Dyn.* **2** (4), 325–355.

SUBRAMANIAN, P., SUJITH, R.I. & WAHI, P. 2013 Subcritical bifurcation and bistability in thermoacoustic systems. *J. Fluid Mech.* **715**, 210–238.

TAKENS, F. 1981 Detecting strange attractors in turbulence. *Lect. Notes Math.* **898**, 366–381.

TATHAWADEKAR, N., DOAN, N.A.K., SILVA, C.F. & THUEREY, N. 2021 Modeling of the nonlinear flame response of a Bunsen-type flame via multi-layer perceptron. *Proc. Combust. Inst.* **38** (4), 6261–6269.

USHAKOV, O.V., WÜNSCHE, H.J., HENNEBERGER, F., KHOVANOV, I.A., SCHIMANSKY-GEIER, L. & ZAKS, M.A. 2005 Coherence resonance near a Hopf bifurcation. *Phys. Rev. Lett.* **95**, 123903.

XU, K. & DARVE, E. 2021 Solving inverse problems in stochastic models using deep neural networks and adversarial training. *Comput. Meth. Appl. Mech. Engng* **384**, 113976.

ZHANG, M., LI, Q. & LIU, J. 2023 On stability and regularization for data-driven solution of parabolic inverse source problems. *J. Comput. Phys.* **474**, 111769.

ZHU, W.Q. & YU, J.S. 1987 On the response of the Van der Pol oscillator to white noise excitation. *J. Sound Vib.* **117** (3), 421–431.

ZHU, Y., GUPTA, V. & LI, L.K.B. 2017 Onset of global instability in low-density jets. *J. Fluid Mech.* **828**, R1.